Journal of Biomechanics ∎ (∎∎∎∎) ∎∎∎–∎∎∎

Contents lists available at ScienceDirect

Journal of Biomechanics

journal homepage: www.elsevier.com/locate/jbiomech
www.JBiomech.com

Hemodynamics of patient-specific aorta-pulmonary shunt configurations

Senol Piskin [a], H. Firat Altin [b], Okan Yildiz [b], Ihsan Bakir [b], Kerem Pekkan [a,c,*]

[a] Department of Biomedical Engineering, Koc University, Istanbul, Turkey
[b] Istanbul Mehmet Akif Ersoy Thoracic and Cardiovascular Surgery Training & Research Hospital, Istanbul, Turkey
[c] Department of Biomedical Engineering, Carnegie Mellon University, Pittsburgh, USA

ARTICLE INFO

Article history:
Accepted 2 November 2016

Keywords:
Hemodynamics
Cardiovascular fluid mechanics
BT shunt configurations
Energy loss
Surgery performance

ABSTRACT

Optimal hemodynamics in aorta-pulmonary shunt reconstruction is essential for improved post-operative recovery of the newborn congenital heart disease patient. However, prior to *in vivo* execution, the prediction of post-operative hemodynamics is extremely challenging due to the interplay of multiple confounding physiological factors. It is hypothesized that the post-operative performance of the surgical shunt can be predicted through computational blood flow simulations that consider patient size, shunt configuration, cardiac output and the complex three-dimensional disease anatomy. Utilizing only the routine patient-specific pre-surgery clinical data sets, we demonstrated an intelligent decision-making process for a real patient having pulmonary artery atresia and ventricular septal defect. For this patient, a total of 12 customized candidate shunt configurations are contemplated and reconstructed virtually using a sketch-based computer-aided anatomical editing tool. Candidate shunt configurations are evaluated based on the parameters that are computed from the flow simulations, which include 3D flow complexity, outlet flow splits, shunt patency, coronary perfusion and energy loss. Our results showed that the modified Blalock-Taussig (mBT) shunt has 12% higher right pulmonary artery (RPA) and 40% lower left pulmonary artery (LPA) flow compared to the central shunt configuration. Also, the RPA flow regime is distinct from the LPA, creating an uneven flow split at the pulmonary arteries. For all three shunt sizes, right mBT innominate and central configurations cause higher pulmonary artery (PA) flow and lower coronary artery pressure than right and left mBT subclavian configurations. While there is a trade-off between energy loss, flow split and coronary artery pressure, overall, the mBT shunts provide sufficient PA perfusion with higher coronary artery pressures and could be preferred for similar patients having PA overflow risk. Central shunts would be preferred otherwise particularly for cases with very low PA overflow risk.

1. Introduction

Pulmonary atresia with ventricular septal defect (PA-VSD) accounts for 1% to 2% of children born with a congenital heart defect. This complex condition differs from the standard tetralogy of Fallot due to its obligatory extra-cardiac pulmonary blood flow sources. For patients with diminished pulmonary blood flow, an artificial systemic-to-pulmonary artery shunt is surgically reconstructed. Several templates have been used to create aorta pulmonary conduits, including the modified Blalock-Taussig (mBT), central, right ventricle-to-pulmonary artery, Potts, Waterston/Cooley and reverse BT (Baba et al., 2013) shunts, even though some of them are very rarely used (van Doorn and de Leval, 2006).

Hospital mortality of mBT and central shunt operations are 10.2% and 14.2%, respectively (European Association for Cardio-Thoracic Surgery, 2015), which is significantly higher than other more complex or simpler pediatric pathologies (European Association for Cardio-Thoracic Surgery, 2015). While it is widely accepted that the outcome depends on the balance between the pulmonary and systemic flows (Q_P/Q_S ratio) (Erek et al., 2006), the prediction of the post-operative hemodynamic state is challenging due to the complex relation between the shunt design, patient-specific anatomy, hemodynamics and cardiac output. The state-of-the art surgical decision-making process is founded on experience and constitutes a qualitative trade-off between the confounding performance objectives. For example, the conduit size should be large enough to supply sufficient blood to the pulmonary vascular bed for adequate oxygenation; but in the case of excessive

* Correspondence to: Mechanical Engineering Department, Koç University, Rumelifeneri Yolu, Sariyer, Istanbul, Turkey.
E-mail address: kpekkan@ku.edu.tr (K. Pekkan).

http://dx.doi.org/10.1016/j.jbiomech.2016.11.014
0021-9290/

pulmonary blood flow, pulmonary edema and heart failure may develop. There are other potential complications directly associated with the shunt hemodynamics, including the risk of stenosis or thrombosis of the shunt, distortion of the pulmonary artery, poor coronary perfusion and asymmetric growth of the pulmonary arteries (Waniewski et al., 2005). Customized vascular simulations based on the three-dimensional (3D) reconstruction of the patient-specific vascular anatomy and flow conditions may allow improved flow physics-based decision-making (Marsden, 2013; Pekkan et al., 2008; Piskin et al., 2015). With this in mind, the objective of the present study is to conduct a real-life pre-surgical planning effort for a neonatal patient case, prior to *in vivo* execution.

Computational fluid dynamics (CFD) has been increasingly used to study the effects of the diameter, curvature and angle of the conduits, and the hemodynamics of mBT procedures (Malota et al., 2007; Migliavacca et al., 2000; Sant'Anna et al., 2003; Waniewski et al., 2005). These studies were exclusively conducted on idealized anatomies and only a few incorporated the real neonatal arterial anatomy. Jinlong et al. (2013) and Qian et al. (2010) presented the post-surgery hemodynamics of one specific shunt type (right ventricle to pulmonary artery conduit) without offering any comparison to other possible shunt templates in the context of surgical planning. On the other hand, Bove et al. (2008) compared *idealized* mBT and right ventricle-pulmonary artery shunt configurations. There are studies utilizing advanced boundary conditions assigned to 3D vascular geometries that have shunt connections, lead by MOCHA investigators (Esmaily-Moghadam et al., 2015a, 2015b; Schiavazzi et al., 2015). Among those, studies with patient specific outlet boundary conditions (Arbia et al., 2015) and a model that predicts the growth of the patient anatomy (Corsini et al., 2015) could be highlighted. To our knowledge, this present manuscript describes the first patient-specific case where the entire anatomical data is acquired from a real patient and a large number of shunt configurations are compared prior to surgery.

2. Materials and methods

2.1. Patient data and anatomical reconstruction

Beginning with a cohort of 140 patients who had aorta-pulmonary shunt surgery, a one-year-old male patient born with pulmonary artery atresia with ventricular septal defect (PA-VSD) was retrospectively selected as an adequate surgical planning case study through the approved IRB. Patients without a computer tomography (CT) scan and who did not have both VSD and pulmonary artery atresia were eliminated from this group before selecting our patient.

3D anatomical data from a 256 multi-slice CT detector (Siemens definition, Erlangen, Germany) with 0.6 mm slice interval was reconstructed as in our previous work (Dur et al., 2011; Pekkan et al., 2009; Sundareswaran et al., 2012, 2008). The final arterial geometry and vessel nomenclatures are presented in Fig. 1. Further details are provided in the Supplementary material, Table A.

2.2. In slico design of shunt configurations

Several candidate shunt location configurations were created in the computer using our in house anatomical editing tool (de Zelicourt et al., 2012; Dur et al., 2011; Piskin et al., 2015). Four configurations were selected for the detailed analysis, as illustrated in Fig. 1. Nomenclature and description of shunt types are provided in the caption for Fig. 1. Common shunts with 3.5, 4 and 5 mm diameters were generated for the selected configurations, resulting in a total of $12(=4\times3)$ simulation cases.

2.3. Numerical flow solver

Detailed description of numerical models and CFD methodology are presented in the Supplementary materials (Appendices A–C). We completed verification of the solver (Dur et al., 2011; Pekkan et al., 2008) and boundary conditions as in our previous studies (de Zelicourt et al., 2012; Piskin et al., 2015) and these results are presented in Appendix A. The vascular resistance values were calculated by verifying the pre-surgical patient specific Q_P/Q_S ratios obtained from the clinical echocardiography and catheterization data as detailed in Appendix B. Finally, Appendix C presents the configuration parameters of the 3D fluid dynamics solver.

The biomechanical parameters that quantify the post-operative surgical performance include graft wall shear stress level, moderate and robust directional trans-shunt flow with low gradients, balanced pulmonary artery flow split between the left and right lungs, higher coronary artery pressure level, Q_P/Q_S ratio, total systemic power loss and low vorticity level in the PAs. The surgical options evaluated in this study are based on these parameters that are computed through the simulations.

3. Results

3.1. Pulmonary flow and Q_P/Q_S ratio

Post-operative vital organ perfusion is considered to be the primary clinical performance parameter. For the selected patient, since the right ventricular outflow tract is totally blocked, the shunt flow is particularly critical as it supplies all of the PA flow. Table 1 presents the flow split ratios for different shunt configurations and sizes. These results suggest that RPA/LPA flow is not symmetric in almost all cases. In particular, the central shunt configuration causes non-symmetric pulmonary artery flow in favor of LPA for all shunt sizes studied. For mBT shunts, RPA and LPA flow differ by more than 20%, while it is around 40% for central shunt configurations. For the right mBT innominate shunt, the RPA/LPA ratio approaches to unity as the shunt size increases. As expected, the choice of larger shunt diameters increases the total pulmonary flow but does not alter the PA split significantly. The only exception is the right mBT subclavian shunt, where a 10–15% increase in RPA perfusion is recorded with respect to the smaller shunt diameters. As such, right mBT innominate shunt configuration resulted in a preferential RPA flow. In contrast, the flow favors LPA for the left mBT subclavian shunt. For shunt diameter sizes of 3.5, 4.0 and 5.0 mm, the Q_P/Q_S ratio ranges are 1.3–1.6, 1.4–2.1 and 1.7–3.0, respectively. These ratios are consistent with clinical findings (Driscoll, 1999) and qualitatively validate our CFD simulations. Finally, our results indicate that for a given cardiac output, anatomy and shunt template, a maximum PA flow limit exists, beyond which the PA flow does not increase further, even through larger shunts are employed.

3.2. Hydrodynamic energy loss

The total energy loss (Restrepo et al., 2015) is a quantitative, normalized (Yigit and Pekkan, 2016) index for the hemodynamic efficiency of the shunt configuration and the single-ventricle afterload. As shunt diameter increases, a significant decrease in energy loss is observed for all shunt types (Table 2). This decrease is dramatically high for the central shunt configuration, reaching ~50% when the diameter is changed from 3.5 to 5 mm, whereas for other configurations (mBT), it is less than 30%.

Energy loss values for mBT shunts are higher than the central configurations as they inherently feature a T-shape anastomosis promoting stagnation and swirl. The difference between the shunt configurations is around 15% for the smallest shunt size (3.5 mm) but becomes more significant, reaching 45% for 4 and 5 mm shunts. For a shunt size of 3.5 mm, all mBT type shunt configurations have similar energy loss values. The improved efficiency of central shunts compared to mBT could be due to their shorter conduit length and their anastomosis curvature.

Larger diameter mBT shunts (4 and 5 mm) show significant variations in energy loss, in contrast to the smaller shunt size

Please cite this article as: Piskin, S., et al., Hemodynamics of patient-specific aorta-pulmonary shunt configurations. Journal of Biomechanics (2016), http://dx.doi.org/10.1016/j.jbiomech.2016.11.014

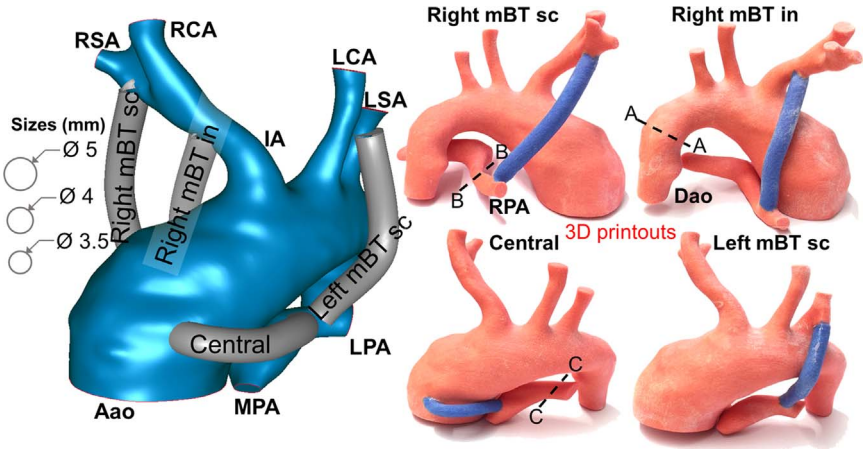

Fig. 1. Three-dimensional reconstructions of the neonatal great arteries and 4 different shunt configurations for the pulmonary artery atresia patient. (LEFT, sagittal plane). Only the largest (5 mm) diameter shunt is displayed, but other sizes studied (3.5 and 4 mm) are provided in scale for comparison. The colored rapid prototypes, shown on RIGHT, are obtained using ProJet 260C 3D (3D Systems, USA), employed for feasibility and risk assessment during pre-surgical planning. Description of the shunt types are as follows; Right mBT innominate (in) configuration connects innominate artery (IA) to right pulmonary artery (RPA). The central shunt is placed between the proximal ascending aorta (Aao) and the main pulmonary artery (MPA). A right modified Blalock-Taussig (mBT) subclavian (sc) shunt connects the right subclavian artery (RSA) to RPA. Finally the left mBT subclavian shunt connects the left subclavian artery (LSA) blood to the left pulmonary artery (LPA). Section A-A indicates aortic isthmus where the mesh convergence of the velocity profile is conducted (Supplementary material, Figure A). Sections B-B and C-C indicate the cross sections where the vortex formation activity are visualized in Figs. 2–5. Dao: Descending aorta, RCA: Right carotid artery, LCA: Left carotid artery.

Table 1
Percent of pulmonary flow split ratios, RPA-LPA and total flow (in parentheses) for all cases studied. All values are normalized by dividing by the maximum total flow (central shunt, diameter of 5 mm).

Configuration Name	3.5 mm	4 mm	5 mm
Right mBT subclavian	36–40 (76)	36–50 (85)	44–53 (96)
Right mBT innominate	39–36 (75)	44–41 (84)	49–49 (97)
Central	31–52 (83)	36–54 (90)	40–60 (100)
Left mBT subclavian	35–41 (76)	37–1 (78)	38–46 (84)

Table 2
Systemic hydrodynamic energy loss, as an indicator of afterload, due to the shunt type employed in [Pa · kg/s] units.

Configuration Name	3.5 mm	4 mm	5 mm
Right mBT Subclavian	62	53	53
Right mBT Innominate	62	57	41
Central	53	44	28
Left mBT Subclavian	61	58	49

Table 3
Relative post-surgery coronary artery pressure levels estimated from the aortic root pressure. Table includes all of the 12 simulation cases. Units are in [mm Hg].

Configuration Name	3.5 mm	4 mm	5 mm
Right mBT Subclavian	46	39	38
Right mBT Innominate	46	42	34
Central	41	36	29
Left mBT Subclavian	46	44	38

(3.5 mm). The right mBT subclavian shunt is the most efficient configuration for the 4 mm diameter, while it is the least efficient for the 5 mm. The left mBT subclavian configuration is the least efficient for the 4 mm diameter shunt size and the right mBT innominate is the most efficient one for the 5 mm shunt. Therefore, for the right mBT subclavian, increasing the shunt diameter will not necessarily improve the energy efficiency, while other shunt types would benefit, due to their monotonous decreasing trend.

3.3. Coronary artery pressure

The use of patient-specific resistance outflow boundary conditions, which represent the characteristics of the downstream vasculature up to the common atrium, allows the correlation of computed aortic root pressure with the coronary artery perfusion. As a critical post-op parameter, the coronary artery perfusion pressures estimated for all shunt configurations are summarized in Table 3. A diastolic pressure above 30 mmHg would be an acceptable limit (Muntner et al., 2004). The central shunts resulted in the lowest coronary perfusion pressure values for all shunt sizes, compared to the mBT. Even the mBT shunt with a 4 mm diameter resulted in higher coronary pressures than the smaller 3.5 mm central shunts.

Shunt configurations with lower energy loss produce lower coronary artery pressures. As the shunt diameter increases, PA flow increases, which results in even lower coronary perfusion pressure levels. Reduced coronary artery pressure could cause myocardial ischemia and infarction, eventually leading to cardiac arrest.

For the 3.5 mm diameter, coronary pressure is almost the same for all mBT configurations. However, for 4 mm, the left mBT subclavian shunt has the highest coronary pressure while the right mBT subclavian has the least among mBT type shunts. For the largest shunt size, this ordering changes and the right mBT innominate results in significantly lower coronary artery pressures.

3.4. 3D flow structures and the PA swirl

Abnormal PA growth is associated with complex flow structures observed in the PAs (Fang et al., 2014; Santoro et al., 2016; Tuchscherer et al., 2007). Our results captured complex swirling flow structures for all shunt configurations and sizes (Figs. 2–5). Vortex formation contributes to the energy dissipation and can partially explain the trends presented in Section 3.2. In general, right mBT configurations (Figs. 2 and 3) tend to produce larger vortex regions compared to the central and left mBT shunt

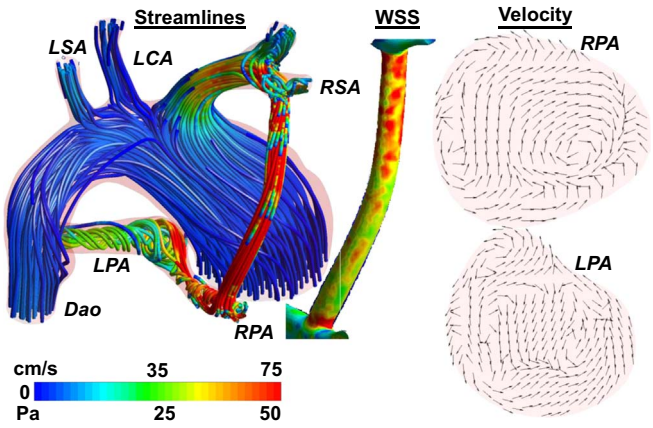

Fig. 2. 3D blood flow streamlines plotted for the 3.5 mm right modified Blalock Taussig (mBT) subclavian shunt configuration. Major vortex formations stabilized at left pulmonary artery (LPA) and right pulmonary artery (RPA) are observed. Corresponding planar velocity vector plots along typical LPA and RPA vessel cross-sections are shown on the RIGHT. Close-up of the wall shear stress (WSS) distribution on the shunt surface and at the anastomosis proximity are also shown. Dao: Descending aorta, RSA: Right subclavian artery, LSA: Left subclavian artery, LCA: Left carotid artery. The upper scale on the color key indicates velocity in cm/s, the lower scale indicates pressure in Pascals.

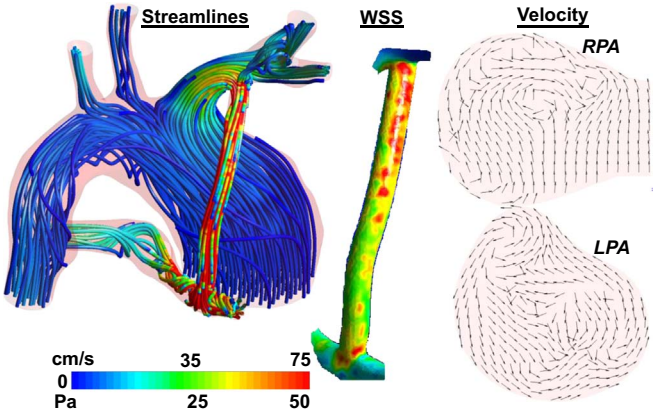

Fig. 3. 3D blood flow streamlines plotted for the 3.5 mm right modified Blalock Taussig (mBT) innominate shunt configuration. Major vortex formations stabilized at left pulmonary artery (LPA) and right pulmonary artery (RPA) are observed. Corresponding planar velocity vector plots along typical LPA and RPA vessel cross-sections are shown on the RIGHT. Close-ups of the wall shear stress (WSS) distribution on the shunt surface and at the anastomosis proximity are also shown.

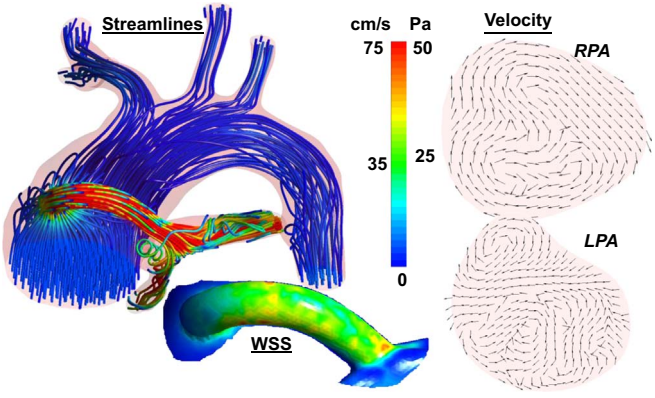

Fig. 4. 3D blood flow streamlines plotted for the 5 mm central shunt configuration. Major vortex formations stabilized at left pulmonary artery (LPA) and right pulmonary artery (RPA) are observed. Corresponding planar velocity vector plots along typical LPA and RPA vessel cross-sections are shown on the RIGHT. Close-ups of the wall shear stress (WSS) distribution on the shunt surface and at the anastomosis proximity are also shown.

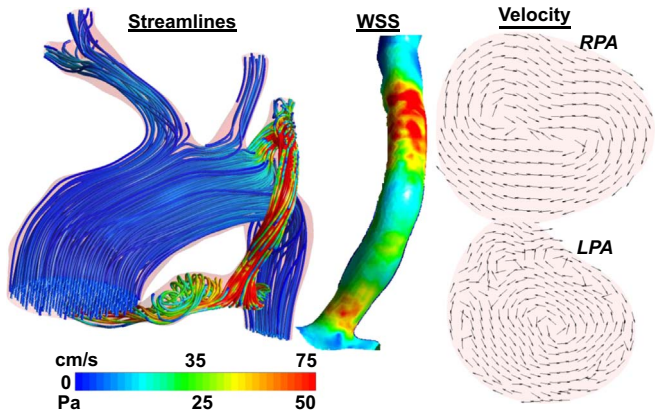

Fig. 5. 3D blood flow streamlines plotted for the 5 mm left modified Blalock Taussig (mBT) subclavian shunt configuration. Major vortex formations stabilized at left pulmonary artery (LPA) and right pulmonary artery (RPA) are observed. Corresponding planar velocity vector plots along typical LPA and RPA vessel cross-sections are shown on the RIGHT. Close-ups of the wall shear stress (WSS) distribution on the shunt surface and at the anastomosis proximity are also shown.

families (Figs. 4 and 5). The formation of PA vortices is highly related to the T-junction topology of shunt anastomosis. Central and left mBT shunt configurations have a relatively smoother anastomosis transition with respect to the direct right mBT type anastomosis, which prevents high vorticity regions. Also, the RPA, which is smaller than the LPA, produces higher vorticity. This finding was verified by computing the total vorticity at pulmonary arteries leading to 1080, 683, 456 and 412 1/s for right mBT innominate, right mBT subclavian, left mBT subclavian and central shunt, respectively.

3.5. Shunt patency and wall shear stress (WSS)

For some configurations, the diseased small diameter PAs draw more than half of the cardiac output, due to the high post-operative Q_P/Q_S ratios encountered (0.9 to 3.0), resulting in high velocity values throughout the shunt and PAs. Thus, the corresponding WSS tends to be higher for mBT type shunt configurations, especially at the shunt and at the systemic anastomosis site (Figs. 2–5). The central shunt configuration has the lowest average WSS among all shunt configurations, even though mBT type shunts showed lower WSS values at some localized points. Very low WSS and sharp WSS changes are prone to plaque formation. Since the central shunt has relatively homogenous WSS distribution, it should be preferred in terms of shunt patency.

4. Discussion

The primary post-operative traumas of aorta-pulmonary shunt operations are associated with underflow, obstruction and overflow. The specific patient analyzed in this study also experienced overflow to the lungs two days into his post-operative term, where a 4 mm right mBT innominate shunt was originally implanted. In order to reduce the PA flow existing major aortapulmonary collateral arteries (MAPCAs) were immediately closed by coiling via catheterization. After this intervention, the only source of PA flow was through the shunt as shown in our computational post-surgical model. The decision about the shunt size and type is mostly based on the clinical experience through a visual comparison with the patient's native vessel size and body weight. Due to the existing ethical regulations authors made sure that the results of the present computations did not influence the decision making process of the surgeon. Still we were able to compare the post-

Please cite this article as: Piskin, S., et al., Hemodynamics of patient-specific aorta-pulmonary shunt configurations. Journal of Biomechanics (2016), http://dx.doi.org/10.1016/j.jbiomech.2016.11.014

operative conditions of the patient with our computational results. The experienced surgeon's decision is fully inline with our computational predictions and provides an encouraging validation case of the present *in silico* approach.

Our results demonstrate that the total PA flow rates of central shunts are significantly higher than the mBT shunt configurations, which would exacerbate the overflow condition if it were adopted for this patient. Furthermore, with a central shunt, the closing of MAPCAs would not be enough to overcome the problem. Likewise, the moderately complex flow patterns of the right mBT innominate shunt provide more symmetric (i.e. balanced) PA perfusion than the central shunt. Although central shunt configurations could be expected to produce a more balanced flow split, the right mBT shunt configuration results in a symmetric flow split between LPA/RPA. This unexpected result is due to a smaller RPA diameter compared to LPA. Thus, patients operated with a right mBT shunt are expected to have less serious post-operative intensive care symptoms due to their more symmetric and low total PA flow rates. Finally, the right or left mBT subclavian configurations proved to be the best for this patient, generating higher coronary artery pressures and coronary artery ischemia was less likely. Therefore, the present results correlate well with the surgical team's original clinical shunt type decision. Although the surgery has been performed with a right mBT innominate shunt, an alternative shunt type (right or left mBT subclavian shunt) likely to work better for the specific patient based on our simulation results (higher coronary artery pressure). The second best, right mBT innominate shunt is still close in performance to right or left mBT subclavian shunt and would be a better option than the central shunt. It is feasible to implement the entire surgical planning pipeline before the execution, in real-time, as it took approximately one day, starting with the patient image data and finishing with the completion of the results report. This approach will enable precise control of Q_P/Q_S through shunt size in a physiologically efficient way. For this patient, a right mBT subclavian shunt, which is commonly used in clinical applications (Ilbawi et al., 1984), with 3.5 and 4 sizes resulted in higher energy loss compared to central shunt.

Central shunt configurations are easier to implant surgically and could be preferred when it is challenging to access the anastomosis sites. In some cases, the necessary vessel could be underdeveloped and might not be suitable for relatively larger (4 or 5 mm) shunts. Furthermore, when conducting subsequent surgeries, the location and dissection of mBT type shunts will be more difficult compared to central shunts. There is another point that makes the central type shunts more advantageous: mBT type shunts cause traction at the pulmonary artery anastomosis region and change the shape and natural development of the pulmonary artery, while these changes are less likely for central type shunts. Moreover, central shunts have shorter graft lengths compared to mBT type shunts, and are thus less likely to close due to hemodynamics after surgery. As such, the central shunt configuration resulted in lower energy dissipation and vorticity levels for this specific patient due to its shorter shunt length. The central shunt configuration could be preferred for patients with underdeveloped myocardium. Quantitative knowledge of the afterload levels of the reconstructed shunts, as predicted here, may allow precise patient-specific customization based on the single-ventricle function.

Although the MAPCAs of the patient have been closed for the current study, the modeling of MAPCAs is an important feature for complete cardiovascular surgery planning. This becomes very important for some patients that are left with residual MAPCAs (intentionally or unintentionally) that are potential to steal significant amount of systemic blood flow. An improved surgical planning model would have to incorporate MAPCAs to the specific generations of the pulmonary artery tree. This can easily be incorporated in the existing arterial-tree resistance boundary condition schemes (Kung et al., 2013). In this approach the flow volume of the MAPCAs can be acquired from the routine patient-specific catheterization or echo measurements prior to surgery.

5. Conclusion

There is no golden-rule for the shunt diameter size and its orientation as these parameters should be decided based on the individual patient. A compromise is needed among the optimal energy loss, pulmonary flow split, smooth PA flow, coronary artery pressure and graft WSS. For larger shunt diameters, energy losses decrease with increased Q_P/Q_S values. Therefore, when higher Q_P/Q_S levels are desired, increasing the size of the shunt diameter is energetically efficient compared to using peripheral vasoconstrictors. The central shunt family produces the highest total PA flow and could be considered for patients without a risk of overflow. If the overflow risk is high, as in the present case, an mBT type shunt could be preferred. If the shunt diameter cannot be larger than 4 mm, the right mBT subclavian configuration should be selected. Otherwise, the right mBT innominate or the left mBT subclavian can be considered. Finally, as the PA flow increases due to shunt configuration, the coronary artery perfusion pressure decreases. The minimum coronary artery pressure that the patient can tolerate needs to be determined based on the peripheral vascular resistances and ventricular function, while also deciding the exact location and size of the shunt.

This study supported the utility of computer simulations in the hemodynamic pre-surgical planning of first-stage shunt surgeries. For the selected patient, this approach was found to be reliable in predicting the possible surgical outcome. More complex cases and surgical scenarios can be evaluated before commencing with the surgery, and the best possible hemodynamic configurations can be determined based on the numerical solutions. The size of the shunt diameter, location and shape of the shunt have a significant effect on the surgical outcome. Patient-specific selection of the critical parameters can optimally condition the patient for planned follow-up surgeries and positively influence the exercise capability. As such, through this approach, the surgeon's decision-making process can be based on scientific evidence in addition to the surgeons' clinical evaluation, resulting in an optimal shunt size and configuration.

Conflict of interest

Authors have no conflict of interest.

Acknowledgements

Funding was provided by grants from the European Research Council (ERC) (Grant No. 641156) Proof of Concept Grant *KidsSurgicalPlan* and EU FP7 293931- *CardioFluidMechanics.*

Appendix A. Supporting information

Supplementary data associated with this article can be found in the online version at http://dx.doi.org/10.1016/j.jbiomech.2016.11.014.

References

Arbia, G., Corsini, C., Baker, C., Pennati, G., Hsia, T.-Y., Vignon-Clementel, I.E., 2015. Pulmonary hemodynamics simulations before stage 2 single ventricle surgery:

patient-specific parameter identification and clinical data assessment. Cardiovasc. Eng. Technol. 6, 268–280.
Baba, K., Honjo, O., Chaturvedi, R., Lee, K.J., Van Arsdell, G., Caldarone, C.A., Benson, L.N., 2013. "Reverse Blalock-Taussig shunt": application in single ventricle hybrid palliation. J. Thorac. Cardiovasc. Surg. 146, 352–357.
Bove, E.L., Migliavacca, F., de Leval, M.R., Balossino, R., Pennati, G., Lloyd, T.R., Khambadkone, S., Hsia, T.Y., Dubini, G., 2008. Use of mathematic modeling to compare and predict hemodynamic effects of the modified Blalock-Taussig and right ventricle-pulmonary artery shunts for hypoplastic left heart syndrome. J. Thorac. Cardiovasc. Surg. 136, 312–320 (e312).
Corsini, C., Baker, C., Baretta, A., Biglino, G., Hlavacek, A.M., Hsia, T.-Y., Kung, E., Marsden, A., Migliavacca, F., Vignon-Clementel, I., Pennati, G., 2015. Integration of clinical data collected at different times for virtual surgery in single ventricle patients: a case study. Ann. Biomed. Eng. 43, 1310–1320.
de Zelicourt, D., Jung, P., Horner, M., Pekkan, K., Kanter, K.R., Yoganathan, A.P., 2012. Cannulation strategy for aortic arch reconstruction using deep hypothermic circulatory arrest. Ann. Thorac. Surg. 94, 614–620.
Driscoll, D.J., 1999. Left-to-right shunt lesions. Pediatric Clinics 46, 355-368.
Dur, O., Coskun, S.T., Coskun, K.O., Frakes, D., Kara, L.B., Pekkan, K., 2011. Computer-aided patient-specific coronary artery graft design improvements using CFD coupled shape optimizer. Cardiovasc. Eng. Technol. 2, 35–47.
Erek, E., Yalcinbas, Y.K., Mamur, Y., Salihoglu, E., Turan, T., Colakoglu, A., Sarioglu, A., Sarioglu, T., 2006. Systemic-to-pulmonary shunt operation in neonates with ductus-dependent pulmonary blood flow. Turk. J. Thorac. Cardiovasc. Surg. 15, 029–035.
Esmaily-Moghadam, M., Hsia, T.Y., Marsden, A.L., 2015a. The assisted bidirectional Glenn: a novel surgical approach for first-stage single-ventricle heart palliation. J. Thorac. Cardiovasc. Surg. 149, 699–705.
Esmaily-Moghadam, M., Murtuza, B., Hsia, T.-Y., Marsden, A., 2015b. Simulations reveal adverse hemodynamics in patients with multiple systemic to pulmonary shunts. J. Biomech. Eng. 137, 0310011–03100112.
European Association for Cardio-Thoracic Surgery, 2015. Mortality vs. Procedure, ⟨http://www.echsacongenitaldb.org/mvp_report/⟩.
Fang, M., Wang, H., Jin, Y., Wang, Z., Wang, Z., Zhang, C., 2014. Development of pulmonary arteries after a central end-to-side shunt in patients with pulmonary atresia, ventricular septal defect, and diminutive pulmonary arteries. Thorac. Cardiovasc. Surg. 62, 211–215.
Ilbawi, M.N., Grieco, J., DeLeon, S.Y., Idriss, F.S., Muster, A.J., Berry, T.E., Klich, J., 1984. Modified Blalock-Taussig shunt in newborn infants. J. Thorac. Cardiovasc. Surg. 88, 770–775.
Jinlong, L., Qi, S., Yi, Q., Haifa, H., Jinfen, L., 2013. Year Numerical simulation and hemodynamic analysis of the modified Blalock-Taussig shunt. In Engineering in Medicine and Biology Society (EMBC) In: Proceedings of the 35th Annual International Conference of the IEEE.
Kung, E., Baretta, A., Baker, C., Arbia, G., Biglino, G., Corsini, C., Schievano, S., Vignon-Clementel, I.E., Dubini, G., Pennati, G., Taylor, A., Dorfman, A., Hlavacek, A.M., Marsden, A.L., Hsia, T.-Y., Migliavacca, F., 2013. Predictive modeling of the virtual Hemi-Fontan operation for second stage single ventricle palliation: two patient-specific cases. J. Biomech. 46, 423–429.
Malota, Z., Nawrat, Z., Kostka, P., 2007. Computer and physical modeling of blood circulation pump support for a new field of application in palliative surgery. Int. J. Artif. Organs 30, 1068–1074.
Marsden, A.L., 2013. Simulation based planning of surgical interventions in pediatric cardiology. Phys. Fluids 25, 101303.
Migliavacca, F., Dubini, G., de Leval, M.R., 2000. Computational fluid dynamics in paediatric cardiac surgery. Images Paediatr. Cardiol. 2, 11–25.
Muntner, P., He, J., Cutler, J.A., Wildman, R.P., Whelton, P.K., 2004. Trends in blood pressure among children and adolescents. Jama 291, 2107–2113.
Pekkan, K., Dur, O., Sundareswaran, K., Kanter, K., Fogel, M., Yoganathan, A., Undar, A., 2008. Neonatal aortic arch hemodynamics and perfusion during cardiopulmonary bypass. J Biomech. Eng. 130, 061012.
Pekkan, K., Dasi, L.P., de Zélicourt, D., Sundareswaran, K.S., Fogel, M.A., Kanter, K.R., Yoganathan, A.P., 2009. Hemodynamic performance of stage-2 univentricular reconstruction: glenn vs. hemi-fontan templates. Ann. Biomed. Eng. 37, 50–63.
Piskin, S., Undar, A., Pekkan, K., 2015. Computational modeling of neonatal cardiopulmonary bypass hemodynamics with full circle of willis anatomy. Artif. organs.
Qian, Y., Liu, J.L., Itatani, K., Miyaji, K., Umezu, M., 2010. Computational hemodynamic analysis in congenital heart disease: simulation of the Norwood procedure. Ann. Biomed. Eng. 38, 2302–2313.
Restrepo, M., Tang, E., Haggerty, C.M., Khiabani, R.H., Mirabella, L., Bethel, J., Valente, A.M., Whitehead, K.K., McElhinney, D.B., Fogel, M.A., Yoganathan, A.P., 2015. Energetic implications of vessel growth and flow changes over time in Fontan patients. Ann. Thorac. Surg. 99, 163–170.
Sant'Anna, J.R.M., Pereira, D.C., Kalil, R.A.K., Prates, P.R., Horowitz, E., Sant'Anna, R.T., Prates, P.R.L., Nesralla, I.A., 2003. Computer dynamics to evaluate blood flow through the modified Blalock-Taussig shunt. Rev. Bras. De. Cir. Cardiovasc. 18, 253–260.
Santoro, G., Capozzi, G., Capogrosso, C., Mahmoud, H.T., Gaio, G., Palladino, M.T., Russo, M.G., 2016. Pulmonary artery growth after arterial duct stenting in completely duct-dependent pulmonary circulation. Heart 102, 459–464.
Schiavazzi, D.E., Kung, E.O., Marsden, A.L., Baker, C., Pennati, G., Hsia, T.Y., Hlavacek, A., Dorfman, A.L., 2015. Hemodynamic effects of left pulmonary artery stenosis after superior cavopulmonary connection: a patient-specific multiscale modeling study. J. Thorac. Cardiovasc. Surg. 149 (689-696), e681–e683.
Sundareswaran, K.S., Pekkan, K., Dasi, L.P., Whitehead, K., Sharma, S., Kanter, K.R., Fogel, M.A., Yoganathan, A.P., 2008. The total cavopulmonary connection resistance: a significant impact on single ventricle hemodynamics at rest and exercise. Am. J. Physiol. - Heart Circ. Physiol. 295, H2427–H2435.
Sundareswaran, K.S., Haggerty, C.M., de Zélicourt, D., Dasi, L.P., Pekkan, K., Frakes, D. H., Powell, A.J., Kanter, K.R., Fogel, M.A., Yoganathan, A.P., 2012. Visualization of flow structures in Fontan patients using 3-dimensional phase contrast magnetic resonance imaging. J. Thorac. Cardiovasc. Surg. 143, 1108–1116.
Tuchscherer, H.A., Vanderpool, R.R., Chesler, N.C., 2007. Pulmonary vascular remodeling in isolated mouse lungs: effects on pulsatile pressure-flow relationships. J Biomech. 40, 993–1001.
van Doorn, C., de Leval, M.R., 2006. Systemic-to-Pulmonary Artery Shunts, Surgery for Congenital Heart Defects. John Wiley & Sons, Ltd, pp. 249–260.
Waniewski, J., Kurowska, W., Mizerski, J.K., Trykozko, A., Nowinski, K., Brzezinska-Rajszys, G., Koscziesza, A., 2005. The effects of graft geometry on the patency of a systemic-to-pulmonary shunt: a computational fluid dynamics study. Artif. Organs 29, 642–650.
Yigit, B., Pekkan, K., 2016. Non-dimensional physics of pulsatile cardiovascular networks and energy efficiency. J. R. Soc., Interface/R. Soc. 13, 20151019.

Please cite this article as: Piskin, S., et al., Hemodynamics of patient-specific aorta-pulmonary shunt configurations. Journal of Biomechanics (2016), http://dx.doi.org/10.1016/j.jbiomech.2016.11.014